On the Properties of Time-Varying SNR Process in Cellular-Enabled UAV Networks

Siva Duggireddy, Pranava C. Stanam, Praful D. Mankar, and Harpreet S. Dhillon

***Abstract*—The unmanned aerial vehicle (UAV) based communication is expected to play an important role in enabling a variety of applications in future cellular networks. However, because of the mobility of the UAVs, the communications links involving UAVs undergo large-scale temporal variations in the received signal quality, which may affect the quality-of-service of the underlying application. Therefore, it is crucial to characterize the time-varying process of signal quality observed by the UAVs. In this paper, we consider a scenario in which a cellular-connected UAV acts as a user equipment (UAV-UE), where the locations of base stations (BSs) follow a Poisson point process (PPP) and the UAV-UE is moving along a 3GPP-inspired straight-line trajectory. For this setting, we study the properties of the *time-varying successful transmission process* that is defined in terms of the time-varying signal-to-noise ratio (SNR) observed at the UAV. In particular, we show that this process is a wide sense stationary (WSS) process and derive its first- and second-order statistics. Finally, we establish an equivalence between the successful transmission processes observed by a UAV-UE served by terrestrial BSs and a terrestrial user served by UAV mounted BSs (UAV-BSs) each moving along an independent straight-line trajectory.**

***Index Terms*—Cellular networks, unmanned aerial vehicle, handover, SNR process, wide sense stationary.**

I. Introduction

Owing to their flexible deployment, UAVs are quickly becoming an integral component of the next generation cellular architecture for enhancing network performance and supporting new applications [1]. For instance, UAV-BSs are useful in enhancing network coverage, improving link reliability and providing additional capacity wherever needed. Besides, UAV-UEs connected with terrestrial BSs are useful for enabling a variety of services such as goods delivery, traffic surveillance, and public safety. In both these cases, the mobility of the UAVs may cause the serving link distance to vary with time, which leads to large-scale variations in the received signal strength. Therefore, it is essential to understand the time-varying performance of the wireless links involving UAVs. Since SNR is one the most fundamental performance measures for wireless links (important on its own right and also an important input for other metrics, such as transmission rate), the primary objective of this paper is to characterize the SNR process for such UAV-assisted communication networks.

Related Works: Owing to their realism in capturing spatial randomness as well as their analytical tractibility, tools from stochastic geometry have been used to study numerous aspects related to the modeling and analysis of UAV-assisted cellular networks over the past few years, e.g., see [2]–[5]. The authors of [2] presented the coverage analysis for a ground user served by the UAV-BSs modeled as a Binomial point process (BPP). The probability of line-of-sight of UAV links in a PPP modeled urban environment is studied in [3]. In [4], the downlink non-orthogonal multiple access of UAV-BSs for the PPP distributed ground users is investigated. Further, a disaster scenario is considered in [5] wherein the UAV-BSs are used in groups for filling voids created by the failure of terrestrial BSs. The coverage probability is analyzed for this setup while assuming that the UAV-BSs follow a clustered point process and the surviving BSs follow a PPP (with reduced density). These analyses provide useful insights into the mean link performance such as coverage probability and spectral efficiency. However, they do not characterize the higher-order properties of the statistical variations in the link quality resulting due to the mobility of UAVs.

Because of mobility, the UAV's serving link distance (thus, the link quality) may exhibits large-scale variations in time which naturally depends on their mobility pattern (or trajectory models). In the literature, a variety of trajectory models have been proposed to accurately model UAV mobility [6]–[8]. Some of the commonly used trajectory models are straight-line, random walk, random waypoint, and Brownian motion [6]. Among these models, straight-line mobility model is the most popular, which has also found applications in the 3GPP studies [9], [10]. The large-scale temporal variations (because of mobility) in link quality give rise to new challenges such as frequent handovers, random sojourn time between handovers, random session rate, time-varying packet service rate, and large-scale variations in received signal strength. The authors of [11] derived the probability of handovers observed by a ground user while assuming that its serving UAV-BSs follow random straight-line trajectories independently of each other. The same authors derived the session rate, defined as the mean rate received in a session time, seen by a ground user in [6] for various trajectory models of UAV-BSs. The authors of [12] derived the sojourn time and handover rate for the straight-line trajectories of UAV-BSs. The rate of handovers with received signal strength based time-to-trigger policy (for avoiding unnecessary handovers due to channel fading) was investigated in [13]. Besides, the authors of [14] derived the association and handover probabilities for 3D multi-tier scenario of UAV-BSs. Most of the works in this direction are focused on the analysis of handover probability and session rate. However,

S. Duggireddy, P. C. Stanam, P. D. Mankar are with SPCRC, IIIT Hyderabad, India (Email: siva.durga@students.iiit.ac.in, spranava.chanakya@research.iiit.ac.in, praful.mankar@iiit.ac.in). H. S. Dhillon is with Wireless@VT, Department of ECE, Virginia Tech, Blacksburg, VA (Email: hdhillon@vt.edu).
The work of H. S. Dillon was supported by US NSF under grant CNS-1923807.

it is surprising to see that the analysis of the time-varying received signal quality of the wireless links involving UAVs remains relatively sparse in the literature. In fact, such analyses are somewhat limited even for the terrestrial networks [15]. This is mainly because of the difficulty in jointly determining the distributions of serving nodes seen by a receiver at two time instances. The authors of [16] presented a joint coverage analysis for a user moving along a straight-line in a terrestrial cellular network modeled as a PPP. For the same setting, the authors of [17] studied the *SNR level crossings process* observed by the moving users and showed that it resembles an alternating-renewal process. In [18], the probability of transmission failure resulting due to the handovers is derived for a terrestrial heterogeneous network with tier-wise biased cell association. Nevertheless, it is important to understand the temporal variations of the SNR process (as a result of the mobility of the UAVs) to gain useful design insights, which is the main topic of this paper.

Contributions: In this paper, we analyze the impact of mobility of a UAV on the SNR-induced transmission process for a cellular-enabled UAV network using stochastic geometry. In particular, we derive the mean and autocorrelation function (ACF) of the successful transmission process while assuming that the locations of the terrestrial BSs follow homogeneous PPP and the UAV-UE follows a straight-line trajectory. We first derive the exact joint distribution of the link distances observed by the UAV at a given time-lag, which is then used to obtain the ACF in the successful transmission process. Using these results, we establish the wide sense stationarity of the successful transmission process. Finally, using the arguments given in [11, Theorem 1], we show that the successful transmission processes observed by a UAV-UE (being served by the terrestrial BS) and a ground UE (being served by UAV-BSs moving along straight lines) are equivalent.

II. System Model

We consider a cellular-enabled UAV network wherein the UAV-UE is being served by the terrestrial BSs. The locations of BSs are assumed to follow a homogeneous PPP Φ of density λ and the UAV-UE is assumed to move at height h (from the ground level) with velocity v in a straight-line oriented in a uniformly random direction θ. We consider the strongest received signal strength based association policy, where the UAV-UE is connected to its nearest BS at any given time. We denote the UAV-UE location using $\tilde{\mathbf{u}}_t$ and its orthogonal projection on the ground using $\mathbf{u}_t$. Thus, the serving link distance at time t becomes $\tilde{R}_t = (h^2 + R_t^2)^{\frac{1}{2}}$ where $R_t = \min_{\mathbf{x}\in\Phi} \|\mathbf{x}-\mathbf{u}_t\|$. Further, we assume the standard power law pathloss model. The SNR at time t is

$$\mathrm{SNR}_t = \frac{\tilde{R}_t^{-\alpha} P}{\sigma_n^2}, \tag{1}$$

where α is pathloss exponent, P is the transmission power, and σ_n^2 is the noise power.

The coverage probability is defined as the probability of observing SNR_t above threshold β and is given by

$$\mathrm{P}_{\mathrm{cov}} = \mathbb{P}[\mathrm{SNR}_t > \beta]. \tag{2}$$

As $\mathrm{P}_{\mathrm{cov}}$ is a spatio-temporally averaged quantity [19], it does not provide information on the higher-order properties of the SNR observed by a UAV-UE while moving along its trajectory. The mobility causes UAV-UE to experience different success probabilities at different times due to the change in its serving link distance. This manifests in temporal variations in the successful transmissions. In order to better understand the impact of these temporal variations on the performance of a UAV-UE, we focus on the statistical characterization of the *successful transmission process*, which is defined next.

Definition 1. *Successful transmission process is defined as*

$$\mathcal{X}_t = \mathbb{1}(\mathrm{SNR}_t > \beta), \tag{3}$$

where $\mathbb{1}(\cdot)$ is the indicator function.

We will focus on determining the first- and second-order statistics of $\mathcal{X}_t$. The mean of $\mathcal{X}_t$ is simply the coverage probability, i.e.,

$$\bar{\mathcal{X}} = \mathbb{E}[\mathbb{1}(\mathrm{SNR}_t > \beta)] = \mathrm{P}_{\mathrm{cov}}, \tag{4}$$

and the ACF of $\mathcal{X}_t$ is

$$\rho_{\mathcal{X}\mathcal{X}}(\tau; t) = \frac{\mathrm{Cov}(\mathcal{X}_t, \mathcal{X}_{t+\tau})}{(\mathrm{Var}(\mathcal{X}_t)\mathrm{Var}(\mathcal{X}_{t+\tau}))^{\frac{1}{2}}}, \tag{5}$$

where $\mathrm{Var}(X)$ is the variance of X and $\mathrm{Cov}(X, Y)$ is the covariance of X and Y.

III. Characterization of $\mathcal{X}_t$

In Section III-B, we will show that the successful transmission process $\mathcal{X}_t$ is a stationary process which in turn allows us to study the behaviour of $\mathcal{X}_t$ at any given time instance, say $t = 0$. For this purpose, we fix the location of the UAV at $\tilde{\mathbf{u}}_o = (o, o, h)$ for $t = 0$, without any loss of generality. Further, by its definition, it is evident that $\mathcal{X}_t$ is completely characterized by the time-varying process of the serving link distance $\tilde{R}_t$. From (1) and (3), it is evident that the correlation coefficient of $\mathcal{X}_o$ and $\mathcal{X}_\tau$ depends on the joint distribution of $\tilde{R}_o$ and $\tilde{R}_\tau$. Hence, we first derive this joint distribution in the following section.

A. Joint Distribution of $\tilde{R}_o$ and $\tilde{R}_\tau$

As $\tilde{R}_o$ and $\tilde{R}_\tau$ are functions of R_o and R_τ, we first determine the joint distribution of R_o and R_τ. Note that $R_o = \|\mathbf{b}_o\|$ and $R_\tau = \|\mathbf{b}_\tau\|$ where $\mathbf{b}_o = \arg\min_{\mathbf{x}\in\Phi} \|\mathbf{x}\|$ and $\mathbf{b}_\tau = \arg\min_{\mathbf{x}\in\Phi} \|\mathbf{x} - \mathbf{u}_\tau\|$ represent nearest BSs to the UAV-UE at time $t = 0$ and $t = \tau$, respectively. Using the *void probability* of PPP, we can directly determine the probability density function (pdf) of R_o as [19]

$$f_{R_o}(r) = 2\pi\lambda r \exp(-\pi\lambda r^2). \tag{6}$$

Let us define $R'_\tau = \|\mathbf{u}_\tau - \mathbf{b}_o\|$. Note that there is at least one handover if the distance of the nearest BS from $\mathbf{u}_\tau$ is below R'_τ at time τ because of the assumption of nearest BS association policy. Let $\mathcal{H}$ and $\mathcal{H}^c$ denote the handover and no handover events, respectively. It is easy to see that $\mathcal{H} \equiv \{\Phi(\mathcal{S}_1) \neq \phi\}$ where $\mathcal{S}_1 = \mathcal{C}_1 \setminus (\mathcal{C}_0 \cap \mathcal{C}_1)$, $\mathcal{C}_0 = \mathcal{B}(R_o, \mathbf{u}_o)$, $\mathcal{C}_1 = \mathcal{B}(R'_\tau, \mathbf{u}_\tau)$ and $\mathcal{B}(r, \mathbf{z})$ is a circle of radius r centered at $\mathbf{z}$. A typical illustration of these circles and set $\mathcal{S}_1$ is depicted

in Fig. 3. Thus, similar to [16, Lemma 1], we can determine the probability of handover within time τ conditioned on R_o and θ using *void probability* of PPP Φ as

$$\mathbb{P}(\mathcal{H}|R_o,\theta) = 1-\exp(-\lambda|\mathcal{S}_1|). \tag{7}$$

where $|\mathcal{S}_1|$ is the Lebesgue measure of set $\mathcal{S}_1$.

Note that the serving link distance at time τ becomes

$$R_\tau = \begin{cases} R'_\tau & \text{when } \mathcal{H}^c \text{ occurs,} \\ \min_{\mathbf{x}\in\Phi}\|\mathbf{x}-\mathbf{u}_\tau\| & \text{when } \mathcal{H} \text{ occurs.} \end{cases} \tag{8}$$

By conditioning on $\mathcal{H}$ and R_o, the cumulative distribution function (CDF) of R_τ is presented in [16, Lemma 2] for the terrestrial cellular networks. Different from this, in the following theorem, we derive the joint distribution of R_o and R_τ by using (8) and appropriately conditioning on $\mathcal{H}$ and $\mathcal{H}^c$.

Theorem 1. *Joint CDF of R_o and R_τ is $F_{R_o,R_\tau}(r_o,r_\tau) =$*

$$\lambda\int_0^{2\pi}\int_0^{r_o} g(u,r_\tau)\exp(-\pi\lambda u^2)u\mathrm{d}u\mathrm{d}\theta, \tag{9}$$

where

$$g(u,r_\tau) = 1-\mathbb{1}[r'_\tau > r_\tau]\exp(-\lambda\mathcal{U}_{v\tau}(r_\tau,u)), \tag{10}$$

$r'_\tau = u^2+v^2\tau^2-2uv\tau\cos(\theta)$ and $\mathcal{U}_{v\tau}(\cdot,\cdot)$ is given in (24)*.*

Proof. Please refer to Appendix A for the proof. □

Using (9), we derive the joint distribution of $\tilde{R}_o$ and $\tilde{R}_\tau$ in the following corollary.

Corollary 1. *Joint CDF of $\tilde{R}_o$ and $\tilde{R}_\tau$ is*

$$F_{\tilde{R}_o,\tilde{R}_\tau}(\tilde{r}_o,\tilde{r}_\tau) = \lambda\int_0^{2\pi}\int_h^{\tilde{r}_o} g(\sqrt{u^2-h^2},\sqrt{\tilde{r}_\tau^2-h^2}) \exp(-\pi\lambda(u^2-h^2))u\mathrm{d}u\mathrm{d}\theta, \tag{11}$$

where $g(\cdot,\cdot)$ is given in (10)*.*

Proof. Please refer to Appendix B for the proof. □

Using the above result, we derive the first- and second-order statistics of $\tilde{R}_t$ and $\mathcal{X}_t$ processes in the next section.

B. Properties of $\tilde{R}_t$ and $\mathcal{X}_t$

In this section, we first show that the process $\tilde{R}_t$ is a WSS process. We then use the similar arguments to establish the WSS property of $\mathcal{X}_t$ and determine its mean and ACF.

Corollary 2. *The process of serving link distance $\tilde{R}_t$ is a WSS process with the mean*

$$\bar{\mathcal{R}} = \frac{1}{2\sqrt{\lambda}}\exp(\pi\lambda h^2), \tag{12}$$

and the ACF

$$\rho_{\tilde{R}\tilde{R}}(\tau) = \frac{4\lambda\exp(-2\pi\lambda h^2)\bar{\mathcal{R}}_2-1}{4\pi\exp(-\pi\lambda h^2)\Gamma(2,\pi\lambda h^2)-1}, \tag{13}$$

where $\Gamma(\cdot,\cdot)$ is the upper incomplete Gamma function and

$$\bar{\mathcal{R}}_2 = \lambda\int_0^{2\pi}\int_h^{\infty} g_1(\tilde{r}_o,\theta)\tilde{r}_o^2\exp\left(-\lambda\pi(\tilde{r}_o^2-h^2)\right)\mathrm{d}\tilde{r}_o\mathrm{d}\theta, \tag{14}$$

such that

$$g_1(\tilde{r}_o,\theta) = h+\int_h^{\tilde{r}'_\tau}\exp(-\lambda(\mathcal{U}_{v\tau}((\tilde{r}_\tau^2-h^2)^{\frac{1}{2}},(\tilde{r}_o^2-h^2)^{\frac{1}{2}}))\mathrm{d}\tilde{r}_\tau,$$

$\tilde{r}'_\tau = ((r'_\tau)^2+h^2)^{\frac{1}{2}}$ and $r'_\tau = r_o^2+v^2\tau^2-2r_ov\tau\cos(\theta)$ and $\mathcal{U}_{v\tau}(\cdot,\cdot)$ is given in (24)*.*

Proof. Please refer to Appendix C for the proof. □

Using (1), we can equivalently describe the process $\mathcal{X}_t$ as

$$\mathcal{X}_t = \mathbb{1}(\tilde{R}_t < \mathrm{R_{th}}),$$

where $\mathrm{R_{th}} = (\beta\sigma_n^2/P)^{-\frac{1}{\alpha}}$. From this, it is evident that the mean of $\mathcal{X}_o$ can be directly obtained using (6) and the correlation of $\mathcal{X}_o$ and $\mathcal{X}_\tau$ can be obtained using the joint distribution of $\tilde{R}_o$ and $\tilde{R}_\tau$ presented in Corollary 1. In fact, in the following theorem, we first argue that the process $\mathcal{X}_t$ is WSS and then determine the mean of $\mathcal{X}_t$ for $t=0$ and ACF of $\mathcal{X}_t$ using the joint distribution of $\tilde{R}_o$ and $\tilde{R}_\tau$.

Theorem 2. *Successful transmission process $\mathcal{X}_t$ is a WSS process with mean*

$$\bar{\mathcal{X}} = \max(0,1-\exp\left(-\lambda\pi(\mathrm{R_{th}}^2-h^2)\right)), \tag{15}$$

and ACF

$$\rho_{\mathcal{X}\mathcal{X}}(\tau) = \frac{F_{\tilde{R}_o,\tilde{R}_\tau}(\mathrm{R_{th}},\mathrm{R_{th}})-\bar{\mathcal{X}}^2}{\bar{\mathcal{X}}(1-\bar{\mathcal{X}})}, \tag{16}$$

where $F_{\tilde{R}_o,\tilde{R}_\tau}(\cdot,\cdot)$ is given in (11)*.*

Proof. Please refer to Appendix D for the proof. □

Corollary 3. *Correlation coefficient $\rho_{\mathcal{X}\mathcal{X}}(\tau)$ is non-negative for all τ.*

Proof. Please refer to Appendix E for the proof. □

Corollary 4. *Successful transmission process $\mathcal{X}_t$ for the following two networks is equivalent:*
1) UAV-UE served by terrestrial BSs: *A network of terrestrial BSs distributed as a homogeneous PPP with density λ and the UAV-UE following a straight-line with velocity v at height h.*
2) UAV-BSs serving terrestrial UE: *A network of UAV-BSs serving a terrestrial user where the UAV-BSs are moving with velocity v in random directions at height h with their initial locations following a 2-D homogeneous PPP of density λ.*

Proof. With small improvisations to the arguments presented in [11, Theorem 1], we can show that successful transmission process $\mathcal{X}_t$ is equivalent for these two setups. □

IV. Numerical Results and Discussion

For numerical results, we consider the following: BS density $\lambda = 10^{-5}$ units/meter^2, UAV flying height $h = 50$ meters, transmission power $P = -30$ dBm, noise power $\sigma_n^2 = -120$ dBm, SNR threshold $\beta = 3$ dB, and pathloss exponent $\alpha = 3$, unless mentioned otherwise.

In Fig. 1, we verify the derived ACF $\rho_{\tilde{R}\tilde{R}}(\tau)$ of the serving link distances using simulation results for velocities $v = \{5,10,20,30\}$ kmph. The lines correspond to the analytical results, whereas the markers correspond to the simulation results. It can be observed that the correlation function is non-negative and decreases with time-lag τ at a higher rate for the higher velocity v. We also observe that the correlation between link distances is independent of the UAV-UE height h. This can

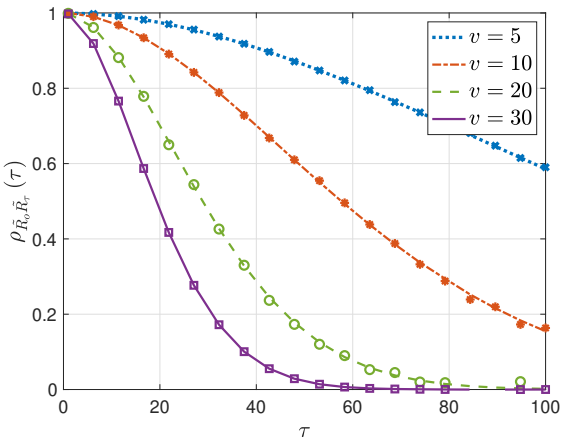

Figure 1. Correlation in $\tilde{R}_o$ and $\tilde{R}_\tau$. The lines correspond to the analytical results, whereas the markers correspond to the simulation results.

be explained by the fact that the correlation is induced by the handovers and the structure of terrestrial Voronoi cells (formed by the PPP distributed BSs), which are both independent of h.

Fig. 2 presents the mean and ACF function of the successful transmission process $\mathcal{X}_t$. From Fig. 2 (Top), it is evident that the mean of $\mathcal{X}_t$ (i.e., the success probability) decreases with increasing height h. This is intuitive as the serving link distance increases with the increase of h. However, the mean of $\mathcal{X}_t$ decreases faster when the pathloss exponent α is higher. This is because a higher α causes a rapid reduction in the received power (or the received SNR), which results in degraded success probability. Moreover, the success probability is zero when h is greater than the distance threshold $\mathrm{R_{th}}$. Besides, note that a better success probability can be observed at higher heights when α is small since $\mathrm{R_{th}}$ is large for a small α.

The ACF of process $\mathcal{X}_t$ is depicted in Fig. 2 (Bottom) for heights $h = \{30, 50\}$ meters and velocities $v = \{5, 10, 20\}$ kmph. It can be observed that the correlation in the successful transmission is significant over a larger time span, especially when velocity v is small. Interestingly, the ACF of $\mathcal{X}_t$ depends on h while the ACF of $\tilde{R}_t$ is independent of h. This is because correlation in $\tilde{R}_t$ is determined by the handover rate and the cell size which are both independent on h (as discussed above) and the correlation in $\mathcal{X}_t$ appears through the condition of successful transmission (i.e., the $\tilde{R}_t \leq \mathrm{R_{th}}$) which is dependent of h.

V. Conclusion

This paper considered a cellular-enabled UAV network wherein terrestrial BSs modeled as a homogeneous PPP serve a UAV-UE that is moving along a randomly oriented straight-line trajectory. For this setup, we have analyzed the SNR-dependent successful transmission process observed by a UAV-UE. As a key enabling result of this analysis, we first derived the joint distribution of the serving link distances seen by the UAV-UE at different time instances. Next, we established that the successful transmission process for this setup is a WSS process. Subsequently, we derived the mean and ACF of this process using the joint distribution of the link distances. Further, we

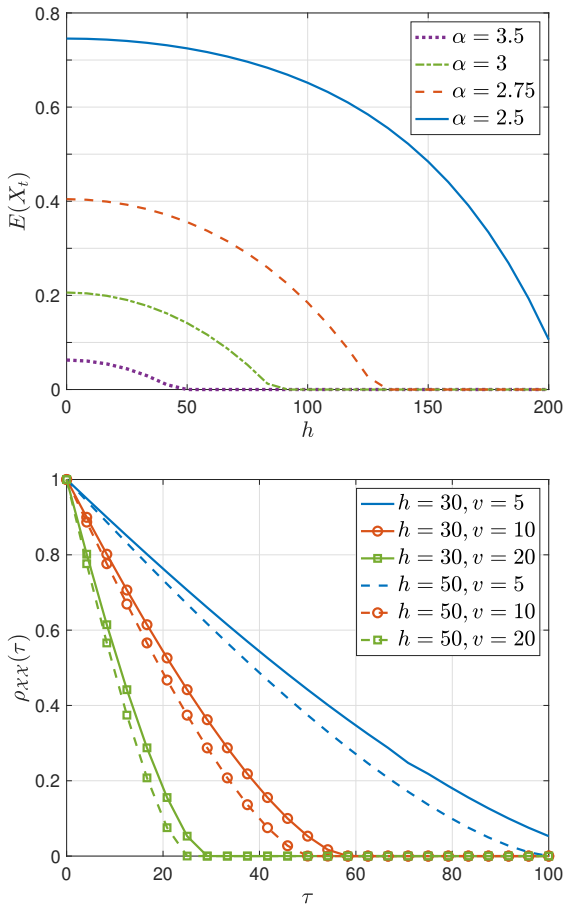

Figure 2. Top: Mean of $\mathcal{X}_t$. Bottom: ACF of $\mathcal{X}_t(\tau)$ for $\alpha = 3$.

have also shown that the successful transmission processes seen by a UAV-UE served by the terrestrial BSs and a terrestrial user served by the UAV-BSs following independent straight-line trajectories are equivalent.

Appendix

A. Proof of Theorem 1

The CDF of R_τ conditioned on R_o and θ is

$$\mathbb{P}(R_\tau \leq r_\tau | R_o, \theta) = \mathbb{P}(R_\tau \leq r_\tau | \mathcal{H}^c, R_o, \theta)\mathbb{P}(\mathcal{H}^c | R_o, \theta) + \mathbb{P}(R_\tau \leq r_\tau | \mathcal{H}, R_o, \theta)\mathbb{P}(\mathcal{H} | R_o, \theta). \quad (17)$$

Let $A = \mathbb{P}(R_\tau \leq r_\tau | \mathcal{H}^c, R_o, \theta)$ and $B = \mathbb{P}(R_\tau \leq r_\tau | \mathcal{H}, R_o, \theta)$. From (8), we know $R_\tau = R'_\tau$ conditioned on $\mathcal{H}^c$. Thus, we have

$$A = \mathbb{1}(R'_\tau < r_\tau), \quad (18)$$

Again from (8), we know that there is at least one BS in the region $\mathcal{S}_1$ conditioned on $\mathcal{H}$, as shown in Fig. 3. Let $\Phi(\mathcal{S}_1) = N$ (number of BSs in $\mathcal{S}_1$). Hence, we can obtain $B =$

$$\mathbb{E}_N\left[\mathbb{P}(R_\tau \leq r_\tau | N)\right] \overset{(a)}{=} 1 - \mathbb{E}_N\left[\mathbb{P}(R_{\tau i} > r_\tau | N)^N\right], \quad (19)$$

where $R_{\tau i} = |\mathbf{u}_\tau - \mathbf{x}_i|$ for $\mathbf{x}_i \in \Phi \cap \mathcal{S}_1$ and step (a) follows from the independence property of PPP. Note that $\mathbf{x}_i$s are uniformly distributed in $\mathcal{S}_1$. Thus, the CDF of $R_{\tau i}$ becomes

$$\mathbb{P}(R_{\tau i} \leq r_\tau) = \frac{|\mathcal{S}_2|}{|\mathcal{S}_1|},$$

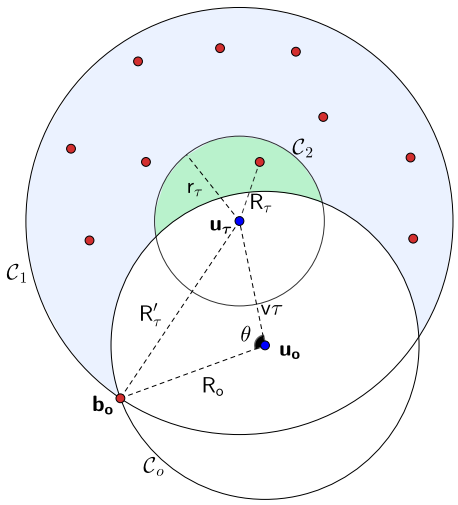

Figure 3. Illustration of handover with link distances R_o and R_τ. $\mathcal{S}_1$ and $\mathcal{S}_2$ are denoted using blue and green shades, respectively, whereas the red and blue dots denote the locations of static BSs and UAV at $t = \{o, \tau\}$, respectively.

where $\mathcal{S}_2 = \mathcal{S}_1 \cap \mathcal{C}_2$, $\mathcal{C}_2 = \mathcal{B}(r_\tau, \mathbf{u}_\tau)$ and $r_\tau \leq R'_\tau$. The regions $\mathcal{S}_1$ and $\mathcal{S}_2$ are illustrated in Fig. 3 using blue and green shades, respectively. Since $\mathcal{S}_2 \subseteq \mathcal{S}_1$ and $\mathcal{S}_1 = \mathcal{C}_1 \setminus (\mathcal{C}_o \cap \mathcal{C}_1)$, we have $\mathcal{S}_2 = \mathcal{C}_2 \setminus (\mathcal{C}_o \cap \mathcal{C}_2)$. To relax the condition $r_\tau \leq R'_\tau$, we can rewrite the CDF of $R_{\tau i}$ as

$$\mathbb{P}(R_{\tau i} \leq r_\tau) = \frac{\min(|\mathcal{S}_2|, |\mathcal{S}_1|)}{|\mathcal{S}_1|}, \text{ for } r_\tau > 0. \tag{20}$$

Condition $\mathcal{H}$ implies that the region $\mathcal{S}_1$ (green region in Fig. 3) is non-empty. Thus, by the definition of the PPP, N follows 0-truncated Poisson distribution with parameter $\lambda|\mathcal{S}_1|$ conditioned on $\mathcal{H}$. Substituting (20) in (19) and then using the moment generating function of distribution of N, we obtain

$$B = 1 - \frac{\exp(-\lambda \min(|\mathcal{S}_2|, |\mathcal{S}_1|)) - \exp(-\lambda|\mathcal{S}_1|)}{1 - \exp(-\lambda|\mathcal{S}_1|)}. \tag{21}$$

Substituting (7), (18) and (21) in (17), we get

$$\begin{aligned}
&\mathbb{P}(R_\tau \leq r_\tau | R_o, \theta) \\
&= \exp(-\lambda|\mathcal{S}_1|)\mathbb{1}\left[R'_\tau \leq r_\tau\right] + 1 - \exp(-\lambda \min(|\mathcal{S}_2|, |\mathcal{S}_1|)), \\
&= 1 + \exp(-\lambda|\mathcal{S}_1|)\mathbb{1}\left[R'_\tau \leq r_\tau\right] - \exp(-\lambda|\mathcal{S}_2|)\mathbb{1}\left[R'_\tau > r_\tau\right] \\
&\quad - \exp(-\lambda|\mathcal{S}_1|)\mathbb{1}\left[R'_\tau \leq r_\tau\right], \\
&= 1 - \exp(-\lambda|\mathcal{S}_2|)\mathbb{1}\left[R'_\tau > r_\tau\right].
\end{aligned} \tag{22}$$

We obtain joint CDF of R_o and R_τ as $F_{R_o,R_t}(r_o, r_\tau) =$

$$\frac{1}{2\pi}\int_0^{2\pi}\int_0^{r_o} \mathbb{P}(R_\tau \leq r_\tau | R_o, \theta) f_{R_o}(u) \mathrm{d}u \mathrm{d}u \mathrm{d}\theta. \tag{23}$$

Now, we provide an expression for calculation of $|\mathcal{S}_i| = |\mathcal{C}_i \setminus (\mathcal{C}_o \cap \mathcal{C}_i)|$ as

$$\mathcal{U}_{v\tau}(r_i, r_o) = \pi r_i^2 - U_{v\tau}(r_i, r_o), \tag{24}$$

where $U_d(r_1, r_2)$ is the area of intersection between two circles of radii r_1 and r_2 with centers separated by distance d. This intersection area can be calculated as

$$U_d(r_1, r_2) = \begin{cases} 0, & \text{for } r_\mathrm{M} + r_\mathrm{n} \leq d, \\ \pi r_\mathrm{n}^2, & \text{for } r_\mathrm{M} - r_\mathrm{n} \geq d, \\ g(r_\mathrm{M}, r_\mathrm{n}, d), & \text{otherwise}, \end{cases}$$

where $r_\mathrm{M} = \max(r_1, r_2)$, $r_\mathrm{n} = \min(r_1, r_2)$ and

$$g(r_\mathrm{M}, r_\mathrm{n}, d) = r_\mathrm{M}^2 \cos^{-1}(d_1/r_\mathrm{M}) - d_1(r_\mathrm{M}^2 - d_1^2)^{\frac{1}{2}} + r_\mathrm{n}^2 \cos^{-1}(d_2/r_\mathrm{n}) - d_2(r_\mathrm{n}^2 - d_2^2)^{\frac{1}{2}}.$$

and $d_1 = \frac{r_\mathrm{M}^2 - r_\mathrm{n}^2 + d^2}{2d}$ and $d_2 = d - d_1$. Finally, substituting (6) and (22) in (23), we obtain (9).

B. Proof of Corollary 1

From (6) and $\tilde{R}_o = (R_o^2 + h^2)^{\frac{1}{2}}$, we can readily obtain

$$f_{\tilde{R}_o}(\tilde{r}_o) = 2\pi\lambda\tilde{r}_o \exp(-\pi\lambda(\tilde{r}_o^2 - h^2)), \tag{25}$$

for $\tilde{r}_o > h$. Besides, we also have $\mathbb{P}(\tilde{R}_\tau \leq \tilde{r}_\tau | \tilde{R}_o = \tilde{r}_o, \theta) =$

$$\mathbb{P}(R_\tau \leq (\tilde{r}_\tau^2 - h^2)^{\frac{1}{2}} | R_o = (\tilde{r}_o^2 - h^2)^{\frac{1}{2}}, \theta). \tag{26}$$

The distribution of R_τ conditioned on R_o and θ is given in (22). Thus, similar to (23), we can write $F_{\tilde{R}_o,\tilde{R}_\tau}(\tilde{r}_o, \tilde{r}_\tau) =$

$$\frac{1}{2\pi}\int_0^{2\pi}\int_0^{\tilde{r}_o} \mathbb{P}(\tilde{R}_\tau \leq \tilde{r_\tau} | \tilde{R}_o = u, \theta) f_{\tilde{R}_o}(u) \mathrm{d}u \mathrm{d}u \mathrm{d}\theta.$$

Finally, substituting (25) and (26) (via (22)) in the above expression, we obtain (11).

C. Proof of Corollary 2

At any given time, the distribution (thus, the mean) of $\tilde{R}_t$ depends on the void probability of $\mathcal{B}((\tilde{r}^2 - h^2)^{\frac{1}{2}}, \mathbf{u}_t)$. However, the void probability for a homogeneous PPP Φ is determined only by the Lebesgue measure of that set and not where it is located. From this, it is apparent that the mean of $\tilde{R}_t$ is independent of t. Further, the correlation of $\tilde{R}_t$ and $\tilde{R}_{t+\tau}$ depends on their joint distribution. As we have seen in Appendix B, this joint distribution is determined by the distribution of points of Φ within the region $\mathcal{S}_1$ that depends on the intersection of $\mathcal{B}((\tilde{R}_t^2 - h^2)^{\frac{1}{2}}, \mathbf{u}_t)$ and $\mathcal{B}((\tilde{R}_{t+\tau}^2 - h^2)^{\frac{1}{2}}, \mathbf{u}_{t+\tau})$. However, the distribution of points of homogeneous PPP Φ in a region is completely determined by its Lebesgue measure. The area of $\mathcal{S}_1$ is determined only by time-lag τ (i.e., the distance travelled by the UAV-UE within time τ). Hence, the ACF of $\tilde{R}_t$ and $\tilde{R}_{t+\tau}$ depends only on τ, and not on t. From these arguments, it is clear that the process $\tilde{R}_t$ is a WSS process. Now, we derive the mean and ACF of $\mathcal{X}_t$.

Since the mean of $\tilde{R}_t$ is independent of t, we can determine it using the pdf of $\tilde{R}_o$ as given in (12). Now, we will obtain ACF $\rho_{\tilde{R}\tilde{R}}$ of process $\tilde{R}_t$ for a given τ at $t = 0$, as it is independent of time. Thus, we have

$$\rho_{\tilde{R}\tilde{R}}(\tau) = \frac{\mathrm{Cov}(\tilde{R}_o, \tilde{R}_\tau)}{(\mathrm{Var}(\tilde{R}_o)\mathrm{Var}(\tilde{R}_\tau))^{\frac{1}{2}}} \overset{(a)}{=} \frac{\mathbb{E}[\tilde{R}_o\tilde{R}_\tau] - \bar{\mathcal{R}}^2}{\mathrm{Var}(\tilde{R}_o)}, \tag{27}$$

where step (a) follows using the fact that $\tilde{R}_o$ and $\tilde{R}_\tau$ are identical in distribution since the serving link distance process is stationary, as discussed above. Using the pdf of $\tilde{R}_o$ given in (25), we can obtain

$$\mathrm{Var}(\tilde{R}_o) = \exp(\pi\lambda h^2)\frac{\Gamma(2, \pi\lambda h^2)}{\pi\lambda} - \frac{1}{4\lambda}\exp(2\pi\lambda h^2). \tag{28}$$

where $\Gamma(\cdot, \cdot)$ is upper incomplete Gamma function. Substituting (12) and (28) in (27) provides (13). Next, we derive the mean of $\tilde{R}_o\tilde{R}_\tau$, defined as $\bar{\mathcal{R}}_2 = \mathbb{E}[\tilde{R}_o\tilde{R}_\tau]$.

Following the similar steps as in Appendix A, we get $\mathbb{E}[\tilde{R}_\tau | \tilde{R}_o, \theta] =$

$$\tilde{R}'_\tau \mathbb{P}(\mathcal{H}^c | \tilde{R}_o, \theta) + \mathbb{E}[\tilde{R}_\tau | \mathcal{H}, \tilde{R}_o, \theta]\mathbb{P}(\mathcal{H} | \tilde{R}_o, \theta). \tag{29}$$

Since $h \leq \tilde{R}_\tau \leq \tilde{R}'_\tau$, we determine $\mathbb{E}[\tilde{R}_\tau|\mathcal{H}, \tilde{R}_o = \tilde{r}_o, \theta]$

$$= h + \int_h^{\tilde{R}'_\tau} \mathbb{P}(\tilde{R}_\tau > \tilde{r}_\tau|\mathcal{H}, \tilde{R}_o = \tilde{r}_o, \theta)\mathrm{d}\tilde{r}_\tau,$$

$$= h + \int_h^{\tilde{R}'_\tau} \mathbb{P}(R_\tau > (\tilde{r}_\tau^2 - h^2)^{\frac{1}{2}}|\mathcal{H}, R_o = (\tilde{r}_o^2 - h^2)^{\frac{1}{2}}, \theta)\mathrm{d}\tilde{r}_\tau,$$

$$\overset{(a)}{=} h + \int_h^{\tilde{R}'_\tau} \frac{\exp(-\lambda|\tilde{\mathcal{S}}_2|) - \exp(-\lambda|\tilde{\mathcal{S}}_1|)}{1 - \exp(-\lambda|\tilde{\mathcal{S}}_1|)}\mathrm{d}\tilde{r}_\tau,$$

where $\tilde{\mathcal{S}}_2 = \tilde{\mathcal{S}}_1 \cap \mathcal{B}((\tilde{r}_\tau^2 - h^2)^{\frac{1}{2}}, \mathbf{u}_\tau)$ and $\tilde{\mathcal{S}}_1 = \tilde{\mathcal{C}}_1 \setminus (\tilde{\mathcal{C}}_1 \cap \tilde{\mathcal{C}}_0)$ (such that $\tilde{\mathcal{C}}_0$ and $\tilde{\mathcal{C}}_1$ are circles of radii $(\tilde{r}_o^2 - h^2)^{\frac{1}{2}}$ and $(\tilde{r}_\tau'^2 - h^2)^{\frac{1}{2}}$). Here, step (a) follows using similar steps used to obtain (21). For a given $\tilde{R}_o = \tilde{r}_o$, we have $\mathbb{P}(\mathcal{H}|\tilde{R}_o, \theta) = 1 - \exp(-\lambda|\tilde{\mathcal{S}}_1|)$. Thus, we can rewrite (29) as

$$\begin{aligned}\mathbb{E}[\tilde{R}_\tau|\tilde{R}_o, \theta] &= \tilde{R}'_\tau \exp(-\lambda|\tilde{\mathcal{S}}_1|) + h[1 - \exp(-\lambda|\tilde{\mathcal{S}}_1|)] \\ &\quad + \int_h^{\tilde{R}'_\tau} \left[\exp(-\lambda|\tilde{\mathcal{S}}_2|) - \exp(-\lambda|\tilde{\mathcal{S}}_1|)\right] \mathrm{d}\tilde{r}_\tau, \\ &\overset{(a)}{=} h + \int_h^{\tilde{R}'_\tau} \exp(-\lambda|\tilde{\mathcal{S}}_2|)\mathrm{d}\tilde{r}_\tau, \end{aligned} \tag{30}$$

where step (a) follows since $\tilde{\mathcal{S}}_1$ does not depend on $\tilde{r}_\tau$. Using this, we can determine the mean of $\tilde{R}_o\tilde{R}_t$ as

$$\bar{\mathcal{R}}_2 = \frac{1}{2\pi}\int_0^{2\pi}\int_h^\infty \tilde{r}_o \mathbb{E}[\tilde{R}_\tau|\tilde{R}_o = \tilde{r}_o, \theta] f_{\tilde{R}_o}(\tilde{r}_o)\mathrm{d}\tilde{r}_o\mathrm{d}\theta.$$

Finally, substituting (25) and (30) in the above expression and further simplifying provides (14).

D. Proof of Theorem 2

Using similar arguments to the ones presented in Appendix C along with $\mathcal{X}_t = \mathbb{1}(\tilde{R}_t \leq \mathrm{R_{th}})$, we can show that the process $\mathcal{X}_t$ is also a WSS process. Now, we derive the mean and ACF of this WSS process. The mean of $\mathcal{X}_t$ can be obtained as

$$\bar{\mathcal{X}} = \mathbb{E}[\mathcal{X}_o] = \mathbb{P}(\tilde{R}_o \leq \mathrm{R_{th}}) = \mathbb{P}(R_o \leq (\mathrm{R_{th}}^2 - h^2)^{\frac{1}{2}}).$$

Note that $\mathbb{E}[\mathcal{X}_\tau] = 0$ if $h > \mathrm{R_{th}}$. Using this and (6), we can obtain the mean of $\mathcal{X}_t$ as given in (15). Next, we obtain the ACF $\rho_{\mathcal{X}\mathcal{X}}$ for a given τ at $t = 0$, as it is independent of t, as

$$\rho_{\mathcal{X}\mathcal{X}}(\tau) = \frac{\mathbb{E}[\mathcal{X}_0\mathcal{X}_\tau] - \mathbb{E}[\mathcal{X}_0]\mathbb{E}[\mathcal{X}_\tau]}{(\mathrm{Var}(\mathcal{X}_0)\mathrm{Var}(\mathcal{X}_\tau))^{\frac{1}{2}}}. \tag{31}$$

Note that $\tilde{R}_o$ and $\tilde{R}_\tau$ are equivalent in distribution because of the homogeneity of PPP Φ, for the reason discussed above. Therefore, we obtain $\mathrm{Var}(\mathcal{X}_o) =$

$$\mathrm{Var}(\mathcal{X}_\tau) = \mathbb{E}[\mathbb{1}(\tilde{R}_o \leq \mathrm{R_{th}})^2] - \bar{\mathcal{X}}^2 = \bar{\mathcal{X}}(1 - \bar{\mathcal{X}}). \tag{32}$$

Now, we can obtain $\mathbb{E}[\mathcal{X}_o\mathcal{X}_\tau] =$

$$\mathbb{E}[\mathbb{1}(\tilde{R}_o \leq \mathrm{R_{th}})\mathbb{1}(\tilde{R}_\tau \leq \mathrm{R_{th}})] = \mathbb{P}(\tilde{R}_o \leq \mathrm{R_{th}}, \tilde{R}_\tau \leq \mathrm{R_{th}}),$$

which is given in (11). Finally, by substituting (11), (15), and (32) in (31), we obtain (16).

E. Proof of Corollary 3

Using (22), we can lower bound the conditional CDF of R_τ as

$$\mathbb{P}(R_\tau \leq r_\tau|R_o, \theta) \geq 1 - \exp(-\lambda\pi r_\tau^2),$$

which is just the marginal distribution of R_τ. Using this, we can lower bound (23) as

$$F_{R_o,R_t}(r_o, r_\tau) \geq F_{R_o}(r_o)F_{R_\tau}(r_\tau).$$

Further extending this result to the joint distribution of $\tilde{R}_o$ and $\tilde{R}_\tau$, we can obtain

$$F_{\tilde{R}_o,\tilde{R}_\tau}(\mathrm{R_{th}}, \mathrm{R_{th}}) \geq F_{\tilde{R}_o}(\mathrm{R_{th}})F_{\tilde{R}_\tau}(\mathrm{R_{th}}) \overset{(a)}{=} \bar{\mathcal{X}}^2,$$

where step (a) follows using $\mathbb{E}[\mathcal{X}_t] = \mathbb{P}(\tilde{R}_o \leq \mathrm{R_{th}})$. From this and (16), we deduce that the correlation coefficient $\rho_{\mathcal{X}\mathcal{X}} \geq 0$.

REFERENCES

[1] M. Mozaffari, W. Saad, M. Bennis, Y.-H. Nam, and M. Debbah, "A tutorial on UAVs for wireless networks: Applications, challenges, and open problems," *IEEE Commun. Surveys Tuts.*, vol. 21, no. 3, pp. 2334–2360, 2019.

[2] V. V. Chetlur and H. S. Dhillon, "Downlink coverage analysis for a finite 3-D wireless network of unmanned aerial vehicles," *IEEE Trans. Commun.*, vol. 65, no. 10, pp. 4543–4558, 2017.

[3] A. Al-Hourani, "On the probability of line-of-sight in urban environments," *IEEE Wireless Commun. Lett.*, vol. 9, no. 8, pp. 1178–1181, 2020.

[4] T. Hou, Y. Liu, Z. Song, X. Sun, and Y. Chen, "Multiple antenna aided NOMA in UAV networks: A stochastic geometry approach," *IEEE Trans. Commun.*, vol. 67, no. 2, pp. 1031–1044, 2019.

[5] A. M. Hayajneh, S. A. R. Zaidi, D. C. McLernon, M. Di Renzo, and M. Ghogho, "Performance analysis of UAV enabled disaster recovery networks: A stochastic geometric framework based on cluster processes," *IEEE Access*, vol. 6, pp. 26 215–26 230, 2018.

[6] M. Banagar and H. S. Dhillon, "Performance characterization of canonical mobility models in drone cellular networks," *IEEE Trans. Wireless Commun.*, vol. 19, no. 7, pp. 4994–5009, 2020.

[7] P. K. Sharma and D. I. Kim, "Random 3D mobile UAV networks: Mobility modeling and coverage probability," *IEEE Transactions on Wireless Communications*, vol. 18, no. 5, pp. 2527–2538, 2019.

[8] S. Enayati, H. Saeedi, H. Pishro-Nik, and H. Yanikomeroglu, "Moving aerial base station networks: A stochastic geometry analysis and design perspective," *IEEE Transactions on Wireless Communications*, vol. 18, no. 6, pp. 2977–2988, 2019.

[9] 3GPP TR-36.777, "Enhanced lte support for aerial vehicles," *Tech. Rep.*, 2018. [Online]. Available: https://portal.3gpp.org/desktopmodules/Specifications/SpecificationDetails.aspx?specificationId=3231

[10] M. Banagar and H. S. Dhillon, "3GPP-inspired stochastic geometry-based mobility model for a drone cellular network," in *IEEE GLOBECOM*, 2019, pp. 1–6.

[11] M. Banagar, V. V. Chetlur, and H. S. Dhillon, "Handover probability in drone cellular networks," *IEEE Wireless Commun. Lett.*, vol. 9, no. 7, pp. 933–937, 2020.

[12] M. Salehi and E. Hossain, "Handover rate and sojourn time analysis in mobile drone-assisted cellular networks," *IEEE Wireless Commun. Lett.*, vol. 10, no. 2, pp. 392–395, 2021.

[13] Y. He, W. Huang, H. Wei, and H. Zhang, "Effect of channel fading and time-to-trigger duration on handover performance in UAV networks," *IEEE Commun. Lett.*, vol. 25, no. 1, pp. 308–312, 2021.

[14] W. Huang, H. Zhang, and M. Zhou, "Analysis of handover probability based on equivalent model for 3D UAV networks," in *2019 IEEE PIMRC*, 2019, pp. 1–6.

[15] H. Tabassum, M. Salehi, and E. Hossain, "Fundamentals of mobility-aware performance characterization of cellular networks: A tutorial," *IEEE Commun. Surveys Tuts.*, vol. 21, no. 3, pp. 2288–2308, 2019.

[16] S. Krishnan and H. S. Dhillon, "Spatio-temporal interference correlation and joint coverage in cellular networks," *IEEE Trans. Wireless Commun.*, vol. 16, no. 9, pp. 5659–5672, 2017.

[17] P. Madadi, F. Baccelli, and G. de Veciana, "On temporal variations in mobile user SNR with applications to perceived qos," in *IEEE WiOpt*, 2016, pp. 1–8.

[18] S. Sadr and R. S. Adve, "Handoff rate and coverage analysis in multi-tier heterogeneous networks," *IEEE Transactions on Wireless Communications*, vol. 14, no. 5, pp. 2626–2638, 2015.

[19] J. G. Andrews, A. K. Gupta, and H. S. Dhillon, "A primer on cellular network analysis using stochastic geometry," 2016. [Online]. Available: https://arxiv.org/abs/1604.03183